HHS Public Access

Author manuscript

Langmuir. Author manuscript; available in PMC 2016 May 12.

Published in final edited form as:

Langmuir. 2015 May 12; 31(18): 5093–5104. doi:10.1021/la504923j.

Phospholipid Composition Modulates Carbon Nanodiamond-Induced Alterations in Phospholipid Domain Formation

Aishik Chakraborty[†], **Nicolas J. Mucci**[†], **Ming Li Tan**[†], **Ashleigh Steckley**[†], **Ti Zhang**[‡], **M. Laird Forrest**[‡], and **Prajnaparamita Dhar**[†,*]

[†]Department of Chemical and Petroleum Engineering, The University of Kansas, Lawrence, Kansas 66045, United States

[‡]Department of Pharmaceutical Chemistry, The University of Kansas, Lawrence, Kansas 66045, United States

Abstract

The focus of this work is to elucidate how phospholipid composition can modulate lipid nanoparticle interactions in phospholipid monolayer systems. We report on alterations in lipid domain formation induced by anionically engineered carbon nanodiamonds (ECNs) as a function of lipid headgroup charge and alkyl chain saturation. Using surface pressure vs area isotherms, monolayer compressibility, and fluorescence microscopy, we found that anionic ECNs induced domain shape alterations in zwitterionic phosphatidylcholine lipids, irrespective of the lipid alkyl chain saturation, even when the surface pressure vs area isotherms did not show any significant changes. Bean-shaped structures characteristic of dipalmitoylphosphatidylcholine (DPPC) were converted to multilobed, fractal, or spiral domains as a result of exposure to ECNs, indicating that ECNs lower the line tension between domains in the case of zwitterionic lipids. For membrane systems containing anionic phospholipids, ECN-induced changes in domain packing were related to the electrostatic interactions between the anionic ECNs and the anionic lipid headgroups, even when zwitterionic lipids are present in excess. By comparing the measured size distributions with our recently developed theory derived by minimizing the free energy associated with the domain energy and mixing entropy, we found that the change in line tension induced by anionic ECNs is dominated by the charge in the condensed lipid domains. Atomic force microscopy images of the transferred anionic films confirm that the location of the anionic ECNs in the lipid monolayers is also modulated by the charge on the condensed lipid domains. Because biological membranes such as lung surfactants contain both saturated and unsaturated phospholipids with different lipid headgroup charges, our results suggest that when studying potential adverse effects of nanoparticles on biological systems the role of lipid compositions cannot be neglected.

[*]**Corresponding Author**: prajnadhar@ku.edu.

Supporting Information

TEM images of the ECNs originally suspended in water and organic solvent. Surface pressure vs area per molecule isotherms. Compressibility modulus vs area per molecule isotherms. Analysis of domain size distribution of DPPC:DPPG and DPPC:POPG monolayers. ECN induced alterations in lipid domains. Fluorescent images of DPPC:POPG films. Detailed height analysis within a condensed domain. List of phospholipid combinations studied along with their overall charge and saturation. Particle size analysis of the ECNs in different media relevant to the experimental conditions. The Supporting Information is available free of charge on the ACS Publications website at DOI: 10.1021/la504923j.

Notes

The authors declare no competing financial interest.

Graphical abstract

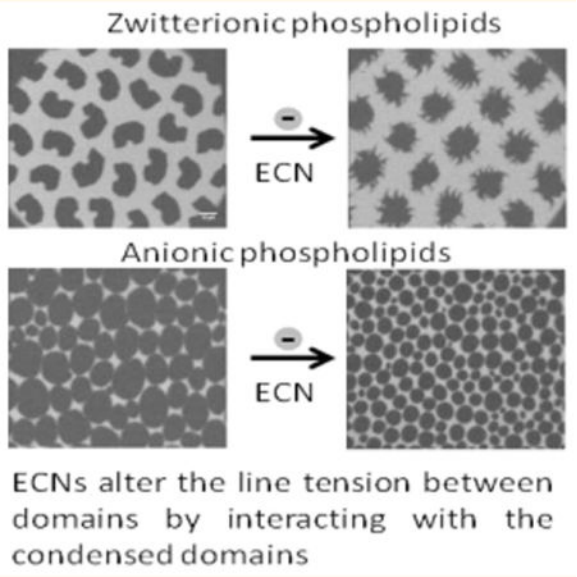

INTRODUCTION

Recent advances in the field of nanotechnology have led to increased use of engineered nanoparticles (ENPs) in commercial applications such as electronic components, cosmetics, surface coatings, and scratch-free paints and biomedical applications such as targeted drug delivery.[1,2] The small size of these engineered nanoparticles leads to altered chemical reactivity when compared to that of their bulk counterparts. Additionally, their extremely small size makes ENPs increasingly capable of entering the human body either through environmental exposure or intentionally by inhalation, ingestion, skin penetration, or being directly injected as in the case of several medical applications. Although their altered chemical reactivity and small size make ENPs desirable for multiple commercial and medical applications, their potential toxic impact on biological materials, living organisms, and the environment is not yet well understood and is therefore a cause for concern.[3]

The respiratory route represents a unique portal of entry for inhaled nanoparticles, resulting in their accumulation in the lung. It has long been known that nanoparticles with a hydrodynamic radius of 10–20 nm are predominantly deposited in the alveolar regions, where they are expected to interact with lung surfactants (LS), a mixture of lipids and proteins that are together responsible for maintaining a low surface tension in the lung and preventing collapse.[4–6] However, an analysis of the nanoparticle deposition has also shown that these smaller nanoparticles are often exhaled during expiration. Rather, nanoparticles and nanoparticle agglomerates in the size range of 0.1–2 μm are more likely to be retained in the alveolar regions.[7,8] As a result, the past few years have seen an increase in studies focused on the biophysical interactions of LS with polymeric and metallic nanoparticles of different composition, size, surface potential, or modified surface chemistry. Unfortunately, many of these studies have demonstrated contradictory effects of the nanoparticles on LS, as summarized below.

Galla and co-workers have reported concentration-dependent adverse effects of hydrophobic polyorganosiloxane (AmOrSil20) on the surface-tension-lowering ability of a model LS. They observed an increased fluidization of the phospholipid monolayers due to interaction with the hydrophobic nanoparticles.[9] In a follow-up article, this group used high-resolution microscopy imaging to further show that the AmOrSil20 nanoparticles influence the insertion of surfactant vesicles into the air/lipid interface in a concentration-dependent manner, possibly by associating with surfactant-associated reservoirs of LS at higher nanoparticle concentrations and surfactant packing[10] while associating with fluid regions of the film at lower surface pressures. More recently, these authors have also provided evidence of the molecular rearrangement of model LS around these hydrophobic nanoparticles,[11] which may also be effected by the size of the hydrophobic nanoparticles.[12] Similarly, Zuo and co-workers have not only demonstrated time-dependent adverse effects of hydroxyapatite nanoparticles on surfactant vesicles of clinical surfactant Infasurf[13] but also have demonstrated a difference in their translocation propensity through lipid monolayers.[14] In contrast, Beck-Broichsitter et al. reported that polystyrene nanoparticles of size 100 nm demonstrated no change in the surface-tension-lowering ability of another clinical surfactant (Alveofact) at a range of different concentrations.[15] Further, Farnoud et al. showed that 200 nm carboxyl-modified polystyrene particles had opposite effects on the packing of dipalmitoylphosphatidylcholine (DPPC) films depending on their mode of exposure. When nanoparticles were injected below a preformed DPPC film, no penetration of the nanoparticles was noted. However, when the phospholipid was spread on a nanoparticle-laden subphase, significant alteration of the DPPC packing was observed. The authors suggest that the sequence of particle and monolayer addition may influence nanoparticle–lipid interactions.[16]

Adverse effects of metallic nanoparticle–lung surfactant lipid interactions on the surface-tension-lowering ability was reported for TiO_2 nanoparticles of size ~5 nm but not for microparticles of TiO_2,[17,18] suggesting that the size of these metallic nanoparticles contributes to their interactions with lipids. Along similar lines, Kodama et al. recently presented evidence of the existence of a critical particle size range that effects the phospholipid domain packing of a model lung surfactant.[19] Bakshi et al. reported that bare gold nanoparticles of size 15 nm impeded the ability of model lung surfactants to lower the surface tension[20] and led to the aggregation of surfactant protein SP-B, preventing efficient adsorption of surfactant to the air/water interface. Contrary to these results, Tatur and Badia demonstrated contrasting behavior in the case of pure or mixed phospholipid monolayers exposed to hydrophobic alkylated gold nanoparticles of average core diameter 2 nm.[21] Their results indicated that even though these functionalized gold nanoparticles did not alter the surface-tension-lowering ability of lung surfactants, they altered the shape and size of liquid-condensed domains in DPPC films, used as a model protein-free LS. Interestingly, no adverse effects were seen for clinical surfactant Survanta[21] (containing both saturated and unsaturated lipids as well as surfactant proteins) even at nanoparticle concentrations that were 2 orders of magnitude higher than in the case of exposure to DPPC. These results suggested that the composition of lipid monolayers and the association of gold nanoparticles with the lipid domains played a dominant role.

The contrasting results of the effect of nanoparticles on phospholipid packing in model lung surfactant function and, particularly, the potential role of surfactant composition on lipid nanoparticle interactions form the major motivations for this study. Although the effects of the shape, size, and surface chemistry of the nanoparticles themselves have been studied in detail, to the best of our knowledge the effect of lipid headgroup charge and lipid saturation on nanoparticle-induced changes in lipid domain formation and lipid packing is currently unknown. Therefore, the focus of this work is to understand how differences in lipid composition alter their interactions with nanoparticles. In particular, we report on the alterations in lipid domain packing of five different lipid compositions with different alkyl chain saturation and headgroup charge (Supporting Information, Table S1) induced by surface-modified engineered carbon nanodiamonds (ECNs) with a net negative charge. The choice of lipids is explained in detail in the Discussion section and aims to reflect the major phospholipid headgroups (phosphatidylcholine, PC; phosphatidylglycerol, PG) in native and synthetic LS mixtures. Because both saturated and unsaturated lipids are essential for the proper functioning of LS, our choice of lipid compositions also reflects the alkyl chain saturations present in LS. ECNs were picked as our choice of nanoparticles because they have recently received a lot of attention as a result of their potential applications in drug delivery, biomedical imaging, and tissue engineering applications[22] and are regularly used by coauthor Forrest for in vivo applications.[23,24] Therefore, understanding the fundamental physical rules governing lipid–nanapoarticle interactions using these nanoparticles is significant from a nanotoxicity perspective.

MATERIALS AND METHODS

Materials

Phospholipids dipalmitoylphosphatidylcholine (DPPC), dipalmitoylphosphatidylglycerol (DPPG), 1-palmitoyl-2-oleoyl-*sn*-glycero-3-phosphocholine (POPC), and 1-palmitoyl-2-oleoyl-*sn*-glycero-3-phospho-(1′-*rac*-glycerol) (POPG) used in this study were purchased from Avanti Polar Lipids (Alabaster, AL) as organic mixtures in chloroform at a final concentration of 5 or 25 mg/mL. Texas red 1,2-dihexadecanoyl-*sn*-glycero-3-phosphoethanolamine, triethylammonium salt, (TXR-DHPE) lipid dye was purchased in the dried form from Life Technologies (Invitrogen, Grand island, NY) and dissolved in high-performance liquid chromatography (HPLC)-grade chloroform (final concentration 0.5 mg/mL). All organic solvents used for this work were purchased from Thermo Fisher Scientific Inc. (Pittsburgh, PA). The subphase water (resistivity 18.2 MΩ/cm) was prepared using a Millipore gradient system (Billerica, MA). The lipid mixtures were stored at −20 °C when not in use to ensure no evaporation of the organic solvent. The carbon nanodiamonds used in this study were obtained from Microdiamant, Lengwil, Switzerland.

Methods

Stock solutions of pure DPPC or DPPG or mixed phospholipids of DPPC:DPPG, DPPC:POPC, and DPPC:POPG in a 70:30 molar ratio for DPPC:POPC and DPPC:POPG and a 75:25 molar ratio for DPPC:DPPG were mixed with 0.5 mol % TXR-DHPE dye in HPLC-grade chloroform:methanol (4:1) mixtures. The ratio of 7:3 was selected primarily because many synthetic lung surfactant mixtures contain this ratio of PG. Stock solutions of

the ECN were prepared by suspending the ECNs initially in water and in the methanol:chloroform mixture and allowing the solution to sonicate for 2 h. Immediately at the end of the sonnication process, the particle size and zeta potential (for the aqueous sample) of the samples were measured using dynamic light scattering (NanoBrook Omni, from Brookhaven Instruments Corporation). The particle size was also measured in the presence of phospholipids in the organic solution. For these samples, stoichiometric volumes of the ECN were added to the organic lipid solution immediately after sonication and used for particle size analysis or for the Langmuir trough experiments described below. Table 1 in the Supporting Information shows the particle size distribution, obtained using the Smoluchowski equation that is built into the software. Our results showed that the carbon nanodiamonds formed aggregates of effective size 219 nm (average of three measurements), with a polydispersity of 0.19 when dispersed in water, whereas the effective size of the aggregates in the organic mixture used for further experiments was found to be 235 nm with a polydispersity of 0.35. Furthermore, we found that this aggregate size did not change within the first half hour after sonnication, ensuring that the particle size did not change during the experiment. The zeta potential was measured using a 1.0 mM KCl solution and was found to be −28 mV. The anionic nature of the ECN surface is a result of the interactions of these nanodiamond powders with air or ozone (during the purification process), which typically results in the presence of COOH groups on the ECN surface.[22] This anionic nature of the ECNs enables several surface modifications that are advantageous for various delivery-based applications.[22]

To initiate each experiment on the Langmuir trough, the lipid/nanoparticle mixture was made in a chloroform:methanol mixture (4:1) and was added dropwise from a Hamilton glass syringe to a water subphase equilibrated to a temperature of 22 °C at a pH of 5.6, contained in a ribbon Langmuir trough (Biolin Scientific Inc.) of maximum area 166 cm^2 and minimum area 46 cm^2. In these experiments, water was chosen as the subphase of choice to eliminate the effect of cations on the phospholipid packing and to compare and contrast our results with previous biophysical measurements using similar phospholipid systems where water was chosen as the subphase.[9,21,25,26] The moveable ribbon allowed controlled compression and expansion of the lipid monolayer formed at the interface, serving as an in vitro model mimicking the change in the alveoli area during inhalation and exhalation. Only the compression cycle is shown here. The trough is computer controlled using the trough control software available at Biolin Scientific. After the sample was spread, the solvent was allowed to evaporate by waiting for 20 min before any compression was started. In this study the monolayer compression rate was kept at 7.0 cm^2/min. This rate is slow enough to allow time for simultaneous focusing on the monolayer film during compression and also mimic a quasistatic compression rate. Compression studies were also conducted at 125 cm^2/min to ensure that the changes in the isotherms were not dependent on the rate of compression. A wet calibrated filter paper was used as a Wilhelmy plate balance allowing continuous recording of the surface pressure during the compression/expansion cycles. The Langmuir trough was mounted on a custom-modified Nikon Eclipse fluorescence microscope with motorized focusing to allow continuous monitoring of the surface morphology during film compression. A 40×-long working distance objective designed for fluorescent light was used to view the lipid monolayer film. A dichroic mirror/

barrier filter assembly directed the excitation light onto the monolayer films at a normal angle of incidence and filtered the emitted light. The images were detected by a fast CCD camera (Andor LUCA), and short image sequences (five frames) were recorded at every 1–5 mN/m surface pressure interval depending on the sample and the surface pressures.

THEORY

Compressibility Modulus

The compressibility of a lipid monolayer is sometimes used to describe the monolayer mechanical properties. The isothermal two-dimensional bulk modulus of a material can be described as the material's ability to store mechanical energy as stress. Mathematically, this two-dimensional bulk modulus, β, is defined as

$$\beta = -A\left(\frac{\partial \Pi}{\partial A}\right)_T = A\left(\frac{\partial \gamma}{\partial A}\right)_T = \frac{1}{\kappa} \quad (1)$$

The inverse of β is defined as the isothermal compressibility, κ, and is often used to quantify mechanical properties of lipid monolayers. Note that β and κ are both second-order derivatives of the free energy, G. $\gamma = (\partial G/\partial A)_T$ and $\beta = (\partial^2 G/\partial A^2)_T$. Therefore, a dip in an experimentally obtained β vs A profile (or a discontinuous change at which $\beta \rightarrow 0$ or $\kappa \rightarrow \infty$) signifies a first-order phase transition. In addition, a higher incompressibility suggests the formation of condensed well-packed films and is essential to the proper functioning of LS. For our experimental results, the compressibility modulus was calculated by taking the derivative of the surface pressure vs area isotherms using built-in functions in Origin 8.62. The data was smoothened using an FFT filter over five points for all points except near the monolayer collapse region.

Calculation of Line Tension Changes from Domain Size Distribution

It is now well known that lipid molecules at the interface undergo lateral organization of the molecules to form domains.[27] Theoretical and experimental work by McConnell and co-workers have shown that the distribution of domain sizes and shape in monolayers is a result of a balance between the interfacial energy at the domain edges (line tension) and electrostatic interactions between domains.[28–30] The difference in lipid chain lengths between the liquid-ordered (l_o) and liquid-disordered (l_d) phases (or liquid condensed (LC) and liquid expanded (LE) phases in the case of monolayers) leads to a line tension, λ, proportional to the hydrophobic mismatch between domains and the interfacial tension of the hydrocarbon–air interface ($\lambda \propto (l_o - l_d)\gamma$). Similarly, a difference in the packing density and composition between lipid phases results in a change in the average dipole density ($\Delta m^2 = m_o - m_d$) due to electrostatic repulsion between and within the domains. This electrostatic repulsion in turn leads to changes in the electrostatic energy of the film. However, these parameters are often difficult to measure, particularly in the presence of small impurities, such as the ECN in this work. We have previously demonstrated a technique to calculate the line tension and dipole density difference of phospholipid domains by comparing the measured size distributions with a theory derived by minimizing the free energy associated with the domain energy and mixing entropy.[31,32] In these systems we assume that the

domains are in equilibrium. Briefly, for a circular domain, the radius of the domain (R) is related to the energy E by the equation

$$\frac{E}{N}=\frac{2a_0}{R}\left[\lambda-\frac{\Delta m^2}{4\pi\varepsilon\varepsilon_o}\ln\left(\frac{4R}{e^2\Delta}\right)\right] \quad (2)$$

In this expression, line tension, λ, between the domains of area a_0 promotes fewer, larger domains, and the dipole density difference, Δm^2, (C/m) between the domains promotes smaller, more numerous domains. Δ is a length on the order of molecular dimensions, ~ 1 nm, ε is the dielectric constant of water (~80), and ε_o is the permittivity of free space (= 8.854×10^{-12} C^2/J m).[28] N is the number of molecules with radius R and can be given by minimizing eq 2, showing that the minimum-energy radius, R_0, for an isolated domain is

$$R_0=\frac{e^3\Delta}{4}\left[\exp\left(\frac{4\pi\varepsilon\varepsilon_o}{\Delta m^2}\lambda\right)\right] \quad (3)$$

However, our results demonstrate that the lipid domains at interfaces are polydisperse and do not alter their shapes for several hours. This observation suggests the role of the entropy of mixing, leading to a domain size distribution. Assuming an ideal entropy of mixing (i.e., no interactions between domains) and equality of the chemical potential of lipid condensed domains of radius R or R_0, we have shown that one can write an equation for the number fractions of domains ($C_{N,M}$) with N (radius R) or M (radius R_0) molecules in terms of the radius of the domains of molecules N and M:[31]

$$C_N=\left[C_M\exp\left\{-\frac{\Delta m^2R_0}{4\varepsilon_o\varepsilon kT}\left(\frac{R_0}{R-1}\right)^2\right\}\right]^{R^2/R_0^2} \quad (4)$$

Equation 4 is used to fit the experimentally obtained domain size distributions, using C_M, $(\Delta m^2R_0)/(4\varepsilon_o\varepsilon kT)$, and R_0 as the three fitting parameters (fits of adjusted r^2 values greater than 0.8 were accepted as good fits). Equation 3 is then used to calculate the line tension.

Image Analysis

All fluorescence microscopy images were analyzed using ImageJ (NIH). To calculate the total change in the packing of the lipid ordered domains, the change (Δ) in the area fraction of the ordered condensed domains (the dark domains in the images) is calculated using the following equation:

$$\Delta\text{condensed area fraction}=\frac{\text{condensed area fraction(control)}-\text{condensed area fraction(w/ECN)}}{\text{condensed area fraction(control)}}$$

where

$$\text{condensed area fraction} = \frac{\text{area of dark domains}}{\text{total area of frame}}$$

The domain size distribution is plotted as normalized histograms with the width of the size distribution being set by dividing the maximum measured domain size by the square root of the number of domains analyzed, $n^{1/2}$. The minimum resolved domain radius was set to be 0.5 μm, which was determined by the resolution of the optical microscope. To improve the statistics, two neighboring frames were analyzed. To represent the histogram as a probability distribution, we represent the number of domains as a relative frequency. Using the nonlinear curve fit feature of Origin 8.6, the domain size distribution of DPPC:DPPG and DPPC:POPG domains with and without ECNs was fit to eq 4, and the fitting parameters were used to calculate the line tension of these monolayers.

Atomic Force Microscopy (AFM)

The location of the ECNs in the anionic lipid monolayers inferred from the domain size distribution of DPPC:DPPG and DPPC:POPG domains with and without ECNs was correlated with high-resolution AFM images of the phospholipid films at a surface pressure of 20 mN/m transferred onto a freshly cleaved mica substrate. A home-built inverse Langmuir–Schaffer technique similar to the technique developed by Lee et al. was used for the film-transfer process.[33] This technique allows the visualization of the film during the transfer process to ensure that there were no perturbations in the domain distribution during the transfer process. Briefly, the mica substrate was placed on an aluminum holder with machined knife edges following the design of Lee et al.[33] This whole apparatus was first thoroughly cleaned and then placed on the bottom of the trough and kept submerged during the compression cycle. When the desired surface pressure was reached, the water was very slowly aspirated until the knife edge cut the monolayer and let it fall onto the substrate. The focus was readjusted throughout the process to ensure that the surface was always visible.

The transferred monolayers were imaged at ambient temperature in air using a Veeco diMultimode V microscope. A J scanner with an *X*–*Y* scan range of 125 × 125 μm^2 was used in tapping mode using antimony-doped silicon probes (Bruker Scientific) with a resonance frequency of 371 kHz. Images were collected at a scan rate of 1 μm/s at a resolution of 512 pixels/line. The images were later flattened using the built-in software to compensate for sample tilt (raised features were excluded from this flattening). The captured images were exported and saved for further use and height analysis.

RESULTS

Isotherms of DPPC

Figure 1A shows a quasi-static surface pressure vs mean molecular area isotherm for a DPPC film containing 1.0 wt % (10 μg/mL) ECN. The averages of three sets are plotted. Surface pressure is defined as $\Pi = \gamma_o - \gamma$, where γ_o = 72 mN/m for water and γ is the measured surface tension. The red dashed line shows a characteristic surface pressure vs mean molecular area of a pure DPPC film. At a very high area per molecule, the monolayer

was in the gas phase, with a nearly zero surface pressure. As the area of the trough was decreased, the total area exposed to the molecules increased, which in turn caused the surface pressure to increase from zero. With increased compression, the film entered the liquid expanded (LE) phase, which was accompanied by a smooth increase in the surface pressure until a plateau was reached at $\Pi = 7$ mN/m, corresponding to the start of the liquid condensed (LC) region. The presence of a plateau region on further compression of the trough was due to an increase in the fraction of LC domains at the expense of the LE phase at a nearly constant surface pressure (coexistence plateau). At the end of this coexistence plateau, the surface pressure increased almost linearly with decreased molecular area until the film underwent collapse at a surface pressure ~72 mN/m. The black dashed–dotted curve shows the measured surface pressure vs mean molecular area after the DPPC film had been incubated with ECN. No significant changes in the collapse surface pressure or the surface pressure corresponding to the LE/LC coexistence plateau were noted when the DPPC solution was incubated with 1.0 wt % (10 μg/mL) ECN. However, the addition of ECN did cause a shift of the curves to smaller mean molecular areas occupied by the lipid molecules, suggesting that the ECNs have a condensing effect on the DPPC domains.

Isotherms of DPPG

Figure 1B shows a typical surface pressure vs mean molecular area isotherm for a DPPG film containing 1.0 wt % (10 μg/mL) ECN. As expected, on the basis of previous reports, a pure DPPG film (red dashed curve) at room temperature did not show an explicit LE/LC coexistence plateau seen for DPPC. Vollhardt et al. showed that this is because DPPG films on a pure water subphase already existed as an LC phase at a surface pressure of 0 mN/m.[25] Upon compression, the surface pressure increased sharply until the film underwent monolayer collapse at a surface pressure of around 60 mN/m. Adding 1.0 wt % (10 μg/mL) ECN did not alter this surface pressure vs area isotherm.

Isotherms of DPPC:DPPG

DPPC:DPPG was used as a model lipid system containing a net negative charge due to the PG headgroup, and the alkyl tail length and tail saturation were the same for both lipids. This model mixture has previously been used by Harishchandra et al. to study the effect of hydrophobic AmOrSil20 on model lipid films. As seen in Figure 1C, the characteristic surface pressure vs mean molecular area isotherm (red dashed curve) resembled that of a pure DPPG film, with no LE/LC coexistence region typical of a DPPC film but had a collapse surface pressure corresponding to a DPPC film. No changes in the pressure area isotherms were observed when 1 wt % (10 μg/mL) ECN was added to this lipid mixture (black dashed–dotted line).

Isotherms of DPPC:POPC

The introduction of unsaturated POPC molecules with mixed alkyl chains alters the ability of DPPC molecules to form well-packed structures. As a result, the addition of POPC significantly alters the surface pressure vs mean molecular area isotherms compared to a characteristic DPPC film. As shown in the red dashed curve in Figure 1D, the LE/LC coexistence plateau was not present at a surface pressure of ~7–9 mN/m; however, a

shoulder appeared at a surface pressure of ~42 mN/m, corresponding to the collapse pressure of pure POPC films. This shoulder corresponds to the “squeeze-out” pressure in LS and causes the pure DPPC film remaining at the interface to reach the ultralow surface pressures desirable for healthy breathing.[31] The black dashed–dotted curve demonstrates the isotherm obtained for DPPC:POPC lipids mixed with 1 wt % (10 μg/mL) ECNs. We found that the surface pressure vs area isotherms obtained overlapped completely with the pure DPPC:POPC system.

Isotherms of DPPC:POPG

Addition of anionic POPG with mixed alkyl chain saturation to the DPPC film caused an increase in both the fluidity of the membrane, as well as a net negatively charged lipid monolayer. Figure 1E (red dashed curve) demonstrates that the LE/LC coexistence was found to occur at a surface pressure of about ~15–17 mN/m. Surface pressure vs mean molecular area isotherms obtained from samples containing 1 wt % (10 μg/mL) ECNs overlapped completely with the characteristic curves of the ECN-free control systems (black dashed–dotted lines).

Compressibility Modulus

Figure 2 shows the compressibility modulus as a function of mean molecular area for all five samples described above. As seen in Figure 2A, at high mean molecular areas (>75 Å^2/molecule), the DPPC film demonstrated a gradual increase in the compressibility modulus to about 25 mN/m followed by a sharp dip at a mean molecular area of about 70 Å^2/molecule. Beyond this dip, the compressibility modulus remained constant at a very small value until it shot up to 190 mN/m corresponding to monolayer collapse. ECN (black dashed curve) did not cause any significant alterations in the compressibility modulus, except at collapse where the maximum compressibility modulus was found to be higher (by 50 mN/m) in case of the lipid film containing ECN. Additionally, the position of the peak compressibility value also shifted to lower mean molecular areas. Figure 2B shows the compressibility modulus for DPPG films before and after adding ECNs. For the control system (red dashed curve), the lack of a significant discontinuity signifies the absence of a first-order phase transition in this system.[25] The addition of ECN showed almost overlapping curves with the control, except for the absolute value of the maximum compressibility modulus, which was higher for the control. Figure 2C shows that for the DPPC:DPPG mixed lipid system no change in the compressibility modulus was observed after adding ECN. Moreover, the position of the maximum shifted to lower mean molecular areas. Figure 2D shows that the compressibility modulus of a DPPC:POPC film (red dashed curve) did not change due to ECNs. Figure 2E shows that no significant changes occur in the DPPC:POPG (red dashed curve) monolayer mechanical properties due to interactions with the ECNs (black dashed–dotted line).

Fluorescent Images of DPPC Monolayers Incubated with ECNs

Figure 3A represents a typical set of images showing the domain morphology of a pure DPPC monolayer at two different surface pressures: 4 mN/m, representative of the LE phase, and 9 mN/m, representative of the LE/LC coexistence phase. In the LE phase,

homogeneous mixing of the lipid dye caused the film to appear uniformly bright. However, this landscape quickly changed with the introduction of ECNs. Images obtained by spreading DPPC solutions mixed with ECN showed clusters of small circular dark domains. The contrast in these images is due to the selective segregation of bulky dye molecules in the more fluid regions, being excluded from the well-packed condensed domains that appear dark.[27,34] In the LE–LC coexistence region, the pure DPPC film showed kidney bean-shaped domains characteristic of DPPC. However, films formed after adding ECNs to the lipid solution started to cause alterations in the domain morphology. The kidney bean-shaped domains started to aggregate to form multilobed structures whereas the net area of condensed LC domains increased, as shown in Figure 6A.

Fluorescence Images of DPPG Monolayers Incubated with ECNs

Figure 3B shows fluorescence microscopy images of DPPG films at two different surface pressures (20 and 30 mN/m) before and after the addition of 10 μg/mL ECNs. The images for the pure DPPG appeared dark because the film exists in an LC state at both of the surface pressures reported.[25] Our images show that adding ECNs caused the DPPG domains to decrease in size, but they were still very well packed. Further analysis of the changes in the LC domains is shown in Figure 6B.

Fluorescence Images of DPPC:DPPG Monolayers Incubated with ECNs

Because the effect of ECN interactions on lipid domain formation were significantly different in DPPC lipids compared to that in anionic DPPG films, we wanted to study what would happen when ECNs were introduced into a system containing both of these lipids. Figure 4 is a representative set of images of our observations. We found that DPPC:DPPG films formed well-packed circular domains. Domains formed by DPPC:DPPG molecules incubated with ECNs showed alterations in the size of the domains and also the domain packing, with more fluid regions being visible. An analysis of the domain size distribution (Supporting Information Figure S4) showed a decrease in the width of the domain size distribution and also a decrease in the minimum-energy radius R_0. Furthermore, Figure 6B shows that in this lipid environment the ECNs induced a significant decrease in the condensed area fraction.

Fluorescence Images of DPPC:POPC Monolayers Incubated with ECNs

To further explore if the alteration in domain packing induced by the ECNs may be modulated by the presence of unsaturated lipids, we also studied the domain formation in a DPPC:POPC film. As noted before, the introduction of phospholipids with mixed alkyl chains such as POPC increased the fluidity of the monolayer when compared to a pure DPPC system, without altering the overall headgroup charge. Figure 5A summarizes our results at two different representative surface pressures (20 and 30 mN/m). The control systems indicate that the kidney bean-shaped domains characteristic of DPPC monolayers were still present, with more bright regions compared to a pure DPPC monolayer. Figure 6 shows that adding ECNs to the lipid solution caused alterations in both the domain shape and domain size distribution. At 30 mN/m, ECNs had an effect similar to that of the pure DPPC system, where the domains developed fractals or spikes arising from the domains.

Furthermore, as shown in Figure 6B, the addition of ECNs to this system caused a decrease in the condensed area fraction of the domains.

Fluorescent Images of DPPC:POPG Monolayers Incubated with ECNs

Finally, to test the effect of both lipid membrane saturation and electrostatic interactions between the anionic lipids and the anionic ECNs, we tested the formation of lipid domains in DPPC:POPG films containing ECNs. The introduction of POPG into DPPC films causes the appearance of circular domains which are not as well packed as films containing disaturated PG lipids, as shown in Figure 5B. It is well known that unlike the DPPC:DPPG system the POPG molecules occupy the more fluid LE phase whereas the DPPC domains make up the LC domains. Although the addition of ECN did not show any visual change in the domain shape or the overall fluidity, an analysis of the domain size distribution (Supporting Information Figure S4) showed that ECNs induced an increase in the minimum-energy domain radius and a decrease in the width of the domain size distribution.

To further analyze the domain morphology of the different lipid systems, due to the presence of the ECN we plot the change in the condensed domain fraction, as shown in Figure 6. A negative change indicates an increase in the total condensed domain fraction, while positive values indicate a decrease. Interestingly, we find that apart from DPPC lipids (Figure 6A) all other lipid mixtures showed a decrease in the net dark domains (Figure 6B), although this value was almost negligible (~5%) for the DPPC:POPG mixture.

We also calculated changes in the line tension of the two anionic lipid mixtures, as shown in Figure 7. We find that the presence of saturated PG lipids causes the ECNs to induce an increase in the line tension, whereas in the presence of unsaturated PG lipids the line tension was found to decrease.

AFM Images of DPPC:DPPG and DPPC:POPG Monolayers Incubated with ECNs

Finally, to correlate the calculated changes in the line tension of the two anionic lipid mixtures with the location of the ECNs in the monolayers, we imaged the DPPC:DPPG and DPPC:POPG films transferred onto a mica substrate at a surface pressure of 20 mN/m. Figure 8 shows higher-resolution images of the lipid domains in the absence (Figure 8A,B) and presence (Figure 8B,D) of ECNs. The light-brown regions correspond to LC domains, and the dark-brown regions correspond to LE regions. The highly ordered lipid tails in LC domains cause LC domains to be slightly higher than the LE regions. Moreover, as noted earlier, the saturated DPPC and DPPG molecules form well-packed LC domains, and the unsaturated POPG lipids occupy LE regions. As a result, Figure 8A shows more LC domains, and the DPPC:POPG film in Figure 8C shows circular but less condensed regions. Furthermore, Figure 8C,D shows the appearance of raised features of height 30–50 nm and size 200 to 400 nm in lipid films containing ECNs. TEM images and DLS measurements described earlier suggest that even though the size of the ECNs in the dry powder state is 5–10 nm, thermodynamics causes these particles to exist as aggregates of size greater than 200 nm. Therefore, in the AFM images, the pink regions of height greater than 20 nm and size greater than 200 nm are attributed to ECNs. A height analysis of some of the raised features in Figure 8C,D (E,F) is also presented for further information on the dimensions of these

raised features. In the case of the DPPC:DPPG films, these large raised features of height greater than 30 nm are away from the domain boundaries, whereas for the DPPC:POPG films these features appear along the domain boundaries. Figure 8C also shows a few raised features within the LC domains. However, a detailed height and size analysis shows that these regions within the LC domains are less than a couple of nanometers high, suggesting that these cannot be ECN aggregates that are composed of spherical or diamond-shaped particles of size 5–10 nm.

DISCUSSION

This research is motivated by the need to understand how lipid headgroup charge and lipid membrane fluidity modulate lipid/nanoparticle interactions leading to alterations in the mechanical and structural properties of lipid monolayers. The effects of both positively and negatively charged nanoparticles on the packing of zwitterionic lipids have been explored both experimentally and theoretically.[35,36] However, to the best of our knowledge, how the lipid membrane packing is altered by charged nanoparticles in zwitterionic, anionic, or mixed zwitterionic/anionic lipids with differences in membrane fluidity is currently not well understood. Our experiments were designed to study both the effect of lipid headgroup charge and lipid chain saturation on lipid nanoparticle interactions. DPPC is the major phospholipid component of LS, and PG lipids form the second most abundant component in native LS. Moreover, native and synthetic LS also contain unsaturated lipids to allow efficient adsorption of LS. Therefore, the lipids used in this study were carefully selected to represent these combinations. Although the studies described here followed changes in the lipid domain packing due to the incubation of lipid molecules with one concentration of ECNs, Supporting Information (Figures S2, S3, and S5) also shows the effect of an order of magnitude higher ECN concentration on these biophysical characteristics. Even though the thermodynamic properties of the lipids are not always significantly affected by the ECNs, both the lipid headgroup charge and lipid alkyl chain saturation can dramatically influence the overall lipid domain shape and size in these systems. Our results conclusively establish that in addition to the surface properties of nanoparticles, the biophysical properties of the lipid compositions can also significantly influence the nanoparticles tendency to alter the phospholipid packing. Below we discuss our results in more detail.

Effect of Lipid Headgroup Charge on Lipid/ECN Interactions in Pure Lipid Systems

DPPC monolayers, with well-characterized monolayer phases, were used as an example of a zwitterionic lipid with a net neutral charge, and DPPG was used as our model anionic lipid. The thermodynamic properties of both of these systems are well characterized. The tail lengths of both of these systems were chosen to be the same to ensure that the difference in lipid/nanoparticle interaction in these two pure systems is only a result of differences in electrostatic interactions between the anionic ECNs and the net neutral or anionic phospholipid headgroups. Although the isotherms for the DPPC films before and after adding ECNs did not show any significant alterations, the compressibility modulus slightly shifted to lower mean molecular areas and showed an increase in the maximum compressibility modulus. This increase implies that exposure to ECNs affected the overall mechanical properties of the DPPC films and caused a possible condensation of the lipid

domains. This possibility was explored further using fluorescence microscopy. Fluorescence microscopy is used to monitor the molecular organization of lipid molecules in lipid monolayers,[27] and the morphology of DPPC monolayers is now well established.[28,37] By comparing the domain morphologies of DPPC films before and after adding ECNs, we found that ECNs caused the early nucleation of lipid domains. Furthermore, an increase in the net condensed area was also measured, further confirming that the ECN caused a condensation of the lipid domains. Such an observation was also reported by Tatur and Badia, even though the physicochemistry of their gold nanoparticles is significantly different from that of our ECNs.[21] We also found that ECNs caused the characteristic bean-shaped domains of zwitterionic DPPC films to form more aggregated multilobed domains. Shape alteration in DPPC films from a kidney bean structure to a more stretched out spiral structure indicates a lowering of the line tension between the LC domains and the surrounding LE regions.[28,38] Such an alteration in domain shape has previously been reported when small amounts of cholesterol were added to a pure DPPC film.[28,39] Galla and co-workers found a similar effect with hydrophobic polymeric nanoparticles,[9] and Tatur and Badia observed a similar effect when studying interactions between alkylated AuNPs and DPPC films, where AFM images showed the presence of aggregates of AuNPs around condensed DPPC domains.[21] The lowering of line tension indicates that like the hydrophobic polymeric and gold nanoparticles, ECNs act as line-active species that prefer to associate with grain boundaries in saturated zwitterionic lipid films, thus altering the phospholipid packing in these systems.

Comparing the results for the effect induced by ECNs on a pure zwitterionic system compared to a pure anionic system such as DPPG, we found that the isotherms and compressibility moduli overlapped completely for the systems with and without ECN, except that a decrease in the maximum compressibility modulus was noted. These observations suggest that the thermodynamic properties of the DPPG films were not affected by exposure to ECN but that the compressibility modulus was decreased, suggesting a slight increase in the membrane fluidity. Similarly, no significant changes were observed in the shape of well-packed large lipid domains of DPPG, after exposure to the ECNs. However, careful analysis of the condensed area fraction did show that ECN induced a decrease (~20%) in the total fraction of dark domains, indicating an increase in the membrane fluidity. McConell and co-workers have previously shown that domain morphologies are determined by a balance between the line tension between domains and electrostatic energies resulting from dipole interactions between domains.[28] The tendency to minimize line tension causes long stretched-out domains, while minimizing dipole interactions causes the breakup of larger domains into smaller sizes. Even though the domains were still well packed for the DPPG films, the decrease in the overall dark condensed domains and the lack of spiral or multilobed domains in the case of pure DPPG suggest that for the pure anionic saturated phospholipid systems these ECNs are no longer line-active species but rather increase the overall fluidity of the monolayers. However, this change was subtle enough that it could not be detected in the compressibility isotherm.

Effect of Lipid Headgroup Charge and Membrane Packing on Lipid/ECN Interactions in Mixed Lipid Systems

To further prove that the differences in the changes in the lipid domain shape and size distribution induced by ECN were due to differences in the interactions with the different lipid headgroups, DPPC:DPPG (7:3) was used as a mixed saturated lipid system. In this system, the LC domains are net negatively charged because of the tendency of DPPG to form LC phases even at very low surface pressure. If our hypothesis, stated above, is correct, then we would expect that the anionic ECNs would be repelled by the anionic LC domains, causing an increase in the membrane fluidity. Furthermore, repulsion from the domain boundaries would cause ECN to increase the line tension because of repulsion from the lipid domain boundary.[31] Indeed, we experimentally measured that the ECNs induced a decrease in the condensed area fraction of domains. We also measured an increase in the line tension between domains for the DPPC:DPPG system, suggesting that the ECNs avoid the line boundaries. To further confirm this, we replaced DPPG with POPG molecules. Because POPG is unsaturated, unlike the DPPG molecules, it is expected to occupy the LE phases in the monolayer.[31] According to our explanation, this would suggest that in the presence of POPG, the ECNs would avoid the fluid LE phases and continue to prefer the condensed DPPC domains, which in turn would cause a lowering of the line tension. Indeed, we do measure a decrease in the line tension between domains for the DPPC:POPG films. This observation is also expected from our previous observations of lipid–protein interactions.[31] We have reported that positively charged proteins caused an increase in line tension between domains in a clinical lung surfactant mixture, where the POPG molecules occupy the fluid LE regions. Finally, our AFM images provide concrete evidence of this hypothesis. Careful analysis of the location of raised features of height 20 nm or greater and sizes greater than 200 nm conclusively established that indeed the submicrometer-sized ECN aggregates prefer the fluid LE phase in the case of the DPPC:DPPG films, while they avoid the anionic LE phase and prefer the LC domain boundaries in the case of the DPPC:POPG films. Furthermore, our Supporting Information shows that at higher ECN concentrations the nanoparticles do cause a visible breaking of the circular domains into spirals, suggesting a further lowering of line tension. Similarly, changing the subphase from water to buffer accentuates the lowering of the line tension in DPPC:POPG films, as shown in the accompanying Supporting Information. Finally, we expect that if the LC domains retain their zwitterionic charge, the ECNs will continue to demonstrate their line-active behavior. Again, this is what was experimentally observed for the DPPC:POPC monolayers. We observed that ECNs caused a decrease in the total condensed area as well, indicating that in the presence of unsaturated lipids the ECNs lose their ability to nucleate and condense the DPPC domains. The reason for this is currently unclear, although one possibility is that at lower surface pressures the ECNs coexist with the unsaturated lipids and are hence unable to serve as nucleation sites for domain condensation. Because the lipid morphology and line tension between domains have been shown to be related to the ability of lung surfactant films to resist collapse at ultralow surface tensions, the potential for readsorption and respreading of lipid material after monolayer collapse, and membrane curvature in lipid bilayers (which in turn can be related to the stability of membranes),[31] we hypothesize that the same nanoparticles can demonstrate significantly different effects on the biophysical performance of different model lipid mixtures. Therefore, our results suggest that when

reporting the potential adverse effects of nanoparticles one should also consider the lipid headgroup charges and alkyl chain saturation and their effects on lipid/nanoparticle interactions.

CONCLUSIONS

We report that phospholipid headgroup charge, lipid composition, and lipid alkyl chain saturation modulate nanoparticle-induced changes in lipid systems. We found that anionic ECNs were line-active and interacted with lipid domain boundaries, resulting in a lowering of line tension, when present in a zwitterionic environment. This observation is in line with prior results with hydrophobic metallic and polymeric particles. In addition, we found that in the presence of anionic phospholipids, electrostatic repulsion between the domains dominated and controlled the alterations in lipid domain packing induced by the ECNs, even in a mixed system with an excess composition of the zwitterionic lipid. Although the effects of nanoparticles of different surface charge, surface modification, and size on the packing of phospholipids have been described before, we present for the first time a controlled study to understand how physicochemical properties of lipids modulate lipid–nanoparticle interactions. Future studies would need to focus on using nanoparticles with different aspect ratios, size, and possibly other physciochemical properties while also varying the lipid composition to obtain a complete biophysical understanding of lipid/nanoparticle interactions in varying lipid environments. Additionally, future studies in our group will also focus on the effect of ionic strength and the presence of ions with different valence on nanoparticle-induced changes in lipid domain packing. A complete understanding of the fundamental physical principles governing lipid–nanoparticle interactions is essential to developing methods to predict the potential adverse effects of ENPs with varied applications.

Supplementary Material

Refer to Web version on PubMed Central for supplementary material.

Acknowledgments

We gratefully acknowledge Dr. Prem Thapa at the University of Kansas Microscopy and Analytical Imaging Facility for obtaining the TEM images. We acknowledge the Bioengineering Research Center (BERC) for access to their AFM. We also acknowledge Mr. Jeff Curley, machinist in the department of chemical and petroleum engineering, for helping us build the stand for the inverse Langmuir–Schaffer transfer. A.C. and P.D. gratefully acknowledge financial support from NIH (P20GM103638) and the Inez Jay Award from Higuchi Biosciences Center. P.D. also acknowledges financial support from the Transportation Research Institute at the University of Kansas.

References

1. Sharifi S, Behzadi S, Laurent S, Forrest ML, Stroeve P, Mahmoudi M. Toxicity of nanomaterials. Chem Soc Rev. 2012; 41:2323–2343. [PubMed: 22170510]
2. Dawson KA, Salvati A, Lynch I. Nanotoxicology: nanoparticles reconstruct lipids. Nat Nanotechnol. 2009; 4:84–85. [PubMed: 19197306]
3. Love SA, Maurer-Jones MA, Thompson JW, Lin YS, Haynes CL. Assessing nanoparticle toxicity. Annu Rev Anal Chem. 2012; 5:181–205.

4. Kapralov AA, Feng WH, Amoscato AA, Yanamala N, Balasubramanian K, Winnica DE, Kisin ER, Kotchey GP, Gou PP, Sparvero LJ, Ray P, Mallampalli RK, Klein-Seetharaman J, Fadeel B, Star A, Shvedova AA, Kagan VE. Adsorption of Surfactant Lipids by Single-Walled Carbon Nanotubes in Mouse Lung upon Pharyngeal Aspiration. ACS Nano. 2012; 6:4147–4156. [PubMed: 22463369]
5. Kendall M, Holgate S. Health impact toxicological effects of nanomaterials in the lung. Respirology. 2012; 17:743–758. [PubMed: 22449246]
6. Schleh C, Kreyling WG, Lehr CM. Pulmonary surfactant is indispensable in order to simulate the in vivo situation. Part Fibre Toxicol. 2013; 1010.1186/1743-8977-10-6
7. Warheit DB. How meaningful are the results of nanotoxicity studies in the absence of adequate material characterization? Toxicol Sci. 2008; 101:183–185. [PubMed: 18300382]
8. Heyder J. Deposition of inhaled particles in the human respiratory tract and consequences for regional targeting in respiratory drug delivery. Proc Am Thorac Soc. 2004; 1:315–20. [PubMed: 16113452]
9. Harishchandra RK, Saleem M, Galla HJ. Nanoparticle interaction with model lung surfactant monolayers. J R Soc Interface. 2010; 7:S15–S26. [PubMed: 19846443]
10. Sachan AK, Harishchandra RK, Bantz C, Maskos M, Reichelt R, Galla HJ. High-resolution investigation of nanoparticle interaction with a model pulmonary surfactant monolayer. ACS Nano. 2012; 6:1677–1687. [PubMed: 22288983]
11. Sachan AK, Galla HJ. Understanding the mutual impact of interaction between hydrophobic nanoparticles and pulmonary surfactant monolayer. Small. 2014; 10:1069–1075. [PubMed: 24339125]
12. Dwivedi MV, Harishchandra RK, Koshkina O, Maskos M, Galla HJ. Size influences the effect of hydrophobic nanoparticles on lung surfactant model systems. Biophys J. 2014; 106:289–298. [PubMed: 24411261]
13. Fan Q, Wang YE, Zhao X, Loo JS, Zuo YY. Adverse biophysical effects of hydroxyapatite nanoparticles on natural pulmonary surfactant. ACS Nano. 2011; 5:6410–6416. [PubMed: 21761867]
14. Hu G, Jiao B, Shi X, Valle RP, Fan Q, Zuo YY. Physicochemical Properties of Nanoparticles Regulate Translocation across Pulmonary Surfactant Monolayer and Formation of Lipoprotein Corona. ACS Nano. 2013; 7:10525–10533. [PubMed: 24266809]
15. Beck-Broichsitter M, Ruppert C, Schmehl T, Guenther A, Betz T, Bakowsky U, Seeger W, Kissel T, Gessler T. Biophysical investigation of pulmonary surfactant surface properties upon contact with polymeric nanoparticles in vitro. Nanomedicine. 2011; 7:341–350. [PubMed: 21059405]
16. Farnoud AM, Fiegel J. Surfactant Interactions with Sub-Micron Particles: The Importance of Route of Exposure. J Aerosol Med Pulm D. 2013; 26:A60–A61.
17. Schleh C, Muhlfeld C, Pulskamp K, Schmiedl A, Nassimi M, Lauenstein HD, Braun A, Krug N, Erpenbeck VJ, Hohlfeld JM. The effect of titanium dioxide nanoparticles on pulmonary surfactant function and ultrastructure. Resp Res. 2009; 1010.1186/1465-9921-10-90
18. Schleh C, Muhlfeld C, Pulskamp K, Schmiedl A, Braun A, Nassimi M, Lauenstein HD, Krug N, Erpenbeck VJ, Hohlfeld JM. Titanium Dioxide Nanoparticles Alter Pulmonary Surfactant Ultrastructure and Biophysical Function. Am J Resp Crit Care Med. 2009; 179:A5255.
19. Kodama AT, Kuo CC, Boatwright T, Dennin M. Investigating the effect of particle size on pulmonary surfactant phase behavior. Biophys J. 2014; 107:1573–1581. [PubMed: 25296309]
20. Bakshi MS, Zhao L, Smith R, Possmayer F, Petersen NO. Metal nanoparticle pollutants interfere with pulmonary surfactant function in vitro. Biophys J. 2008; 94:855–868. [PubMed: 17890383]
21. Tatur S, Badia A. Influence of Hydrophobic Alkylated Gold Nanoparticles on the Phase Behavior of Monolayers of DPPC and Clinical Lung Surfactant. Langmuir. 2012; 28:628–639. [PubMed: 22118426]
22. Mochalin VN, Shenderova O, Ho D, Gogotsi Y. The properties and applications of nanodiamonds. Nat Nanotechnol. 2012; 7:11–23. [PubMed: 22179567]
23. Zhang T, Cui H, Chang H-C, Yang X, ML F. Photoacoustic imaging of biological tissues with radiation damaged nanodiamonds as a near infrared optical contrast agent. J Biomed Opt. 2013; 18:26018. [PubMed: 23400417]

24. Zhang T, Cui H, Fang C-Y, Cheng K, Yang X, Chang H-C, Forrest ML. Targeted nanodiamons as phenotype-specific photoacoustic contrast agents for breast cancer. Nanomedicine. 2015; 10:573–587. [PubMed: 25723091]
25. Vollhardt D, Fainerman VB, Siegel S. Thermodynamic and textural characterization of DPPG phospholipid monolayers. J Phys Chem B. 2000; 104:4115–4121.
26. Farnoud AM, Fiegel J. Interaction of dipalmitoyl phosphatidylcholine monolayers with a particle-laden subphase. J Phys Chem B. 2013; 117:12124–12134. [PubMed: 23987143]
27. Knobler CM. Seeing phenomena in flatland - studies of monolayers by fluorescence microscopy. Science. 1990; 249:870–874. [PubMed: 17773103]
28. Mcconnell HM. Structures and Transitions in Lipid Monolayers at the Air-Water-Interface. Annu Rev Phys Chem. 1991; 42:171–195.
29. Benvegnu DJ, McConnell HM. Line Tension between Liquid Domains in Lipid Monolayers. J Phys Chem. 1992; 96:6820–6824.
30. Benvegnu DJ, McConnell HM. Surface Dipole Densities in Lipid Monolayers. J Phys Chem. 1993; 97:6686–6691.
31. Dhar P, Eck E, Israelachvili JN, Lee DW, Min Y, Ramachandran A, Waring AJ, Zasadzinski JA. Lipid-protein interactions alter line tensions and domain size distributions in lung surfactant monolayers. Biophys J. 2012; 102:56–65. [PubMed: 22225798]
32. Lee DW, Min Y, Dhar P, Ramachandran A, Israelachvili JN, Zasadzinski JA. Relating domain size distribution to line tension and molecular dipole density in model cytoplasmic myelin lipid monolayers. Proc Natl Acad Sci USA. 2011; 108:9425–9430. [PubMed: 21606329]
33. Lee KYC, Lipp MM, Takamoto DY, Ter-Ovanesyan E, Zasadzinski JA, Waring AJ. Apparatus for the continuous monitoring of surface morphology via fluorescence microscopy during monolayer transfer to substrates. Langmuir. 1998; 14:2567–2572.
34. Mohwald H. Phospholipid and phospholipid-protein monolayers at the air/water interface. Annu Rev Phys Chem. 1990; 41:441–476. [PubMed: 2257038]
35. Velikonja A, Santhosh PB, Gongadze E, Kulkarni M, Elersic K, Perutkova S, Kralj-Iglic V, Ulrih NP, Iglic A. Interaction between Dipolar Lipid Headgroups and Charged Nanoparticles Mediated by Water Dipoles and Ions. Int J Mol Sci. 2013; 14:15312–15329. [PubMed: 23887653]
36. Wang B, Zhang LF, Bae SC, Granick S. Nanoparticle-induced surface reconstruction of phospholipid membranes. Proc Natl Acad Sci USA. 2008; 105:18171–18175. [PubMed: 19011086]
37. McConlogue CW, Vanderlick TK. A close look at domain formation in DPPC monolayers. Langmuir. 1997; 13:7158–7164.
38. Keller SL, McConnell HM. Stripe phases in lipid monolayers near a miscibility critical point. Phys Rev Lett. 1999; 82:1602–1605.
39. Kim K, Choi SQ, Zell ZA, Squires TM, Zasadzinski JA. Effect of cholesterol nanodomains on monolayer morphology and dynamics. Proc Natl Acad Sci USA. 2013; 110:E3054–E3060. [PubMed: 23901107]

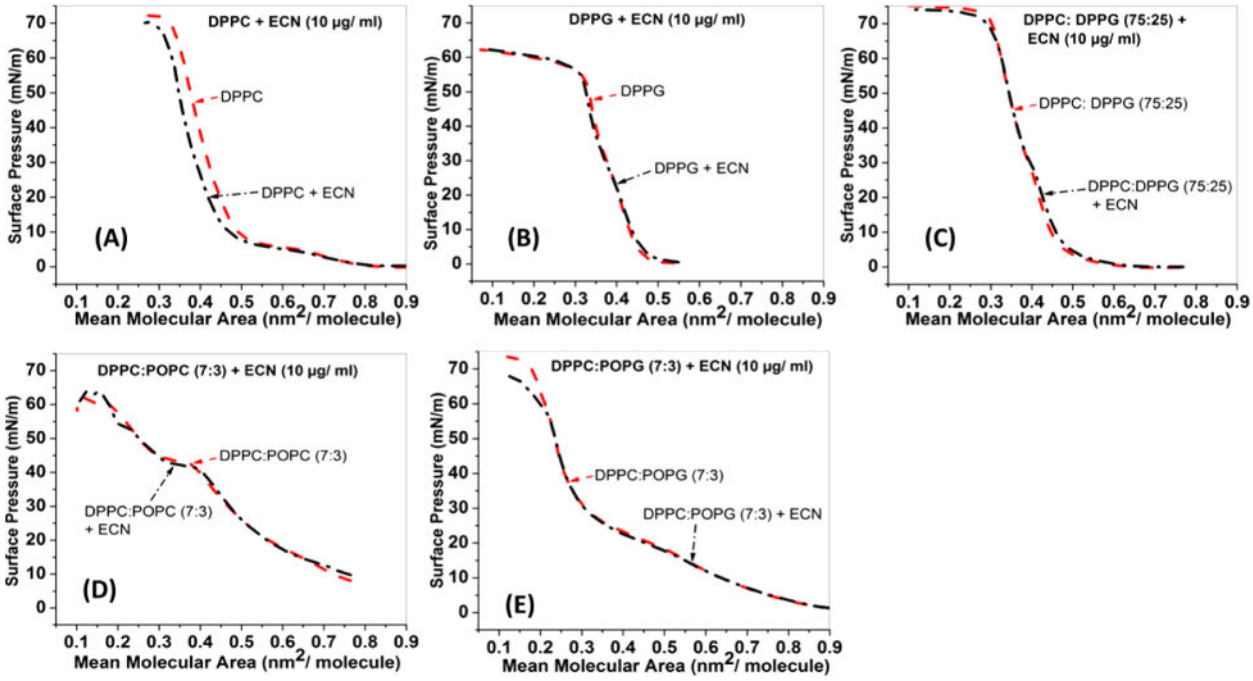

Figure 1.

Surface pressure vs mean molecular area isotherms for (A) DPPC, (B) DPPG, (C) DPPC:DPPG (75:25), (D) DPPC:POPC (7:3), and (E) DPPC:POPG (7:3) monolayers containing 1 wt % (10 *µ*g/mL) ECN.

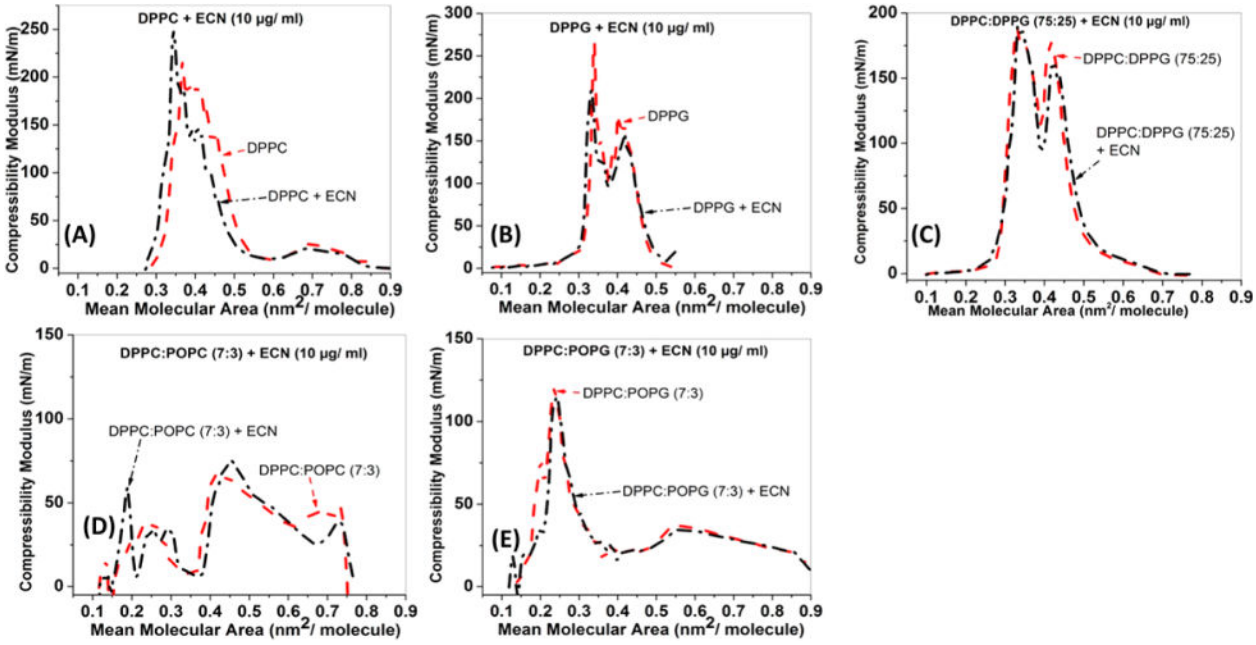

Figure 2.

Compressibility modulus vs mean molecular area isotherms for (A) DPPC, (B) DPPG, (C) DPPC:DPPG (75:25), (D) DPPC:POPC (7:3), and (E) DPPC:POPG (7:3) monolayers containing 1 wt % (10 μg/mL) ECN.

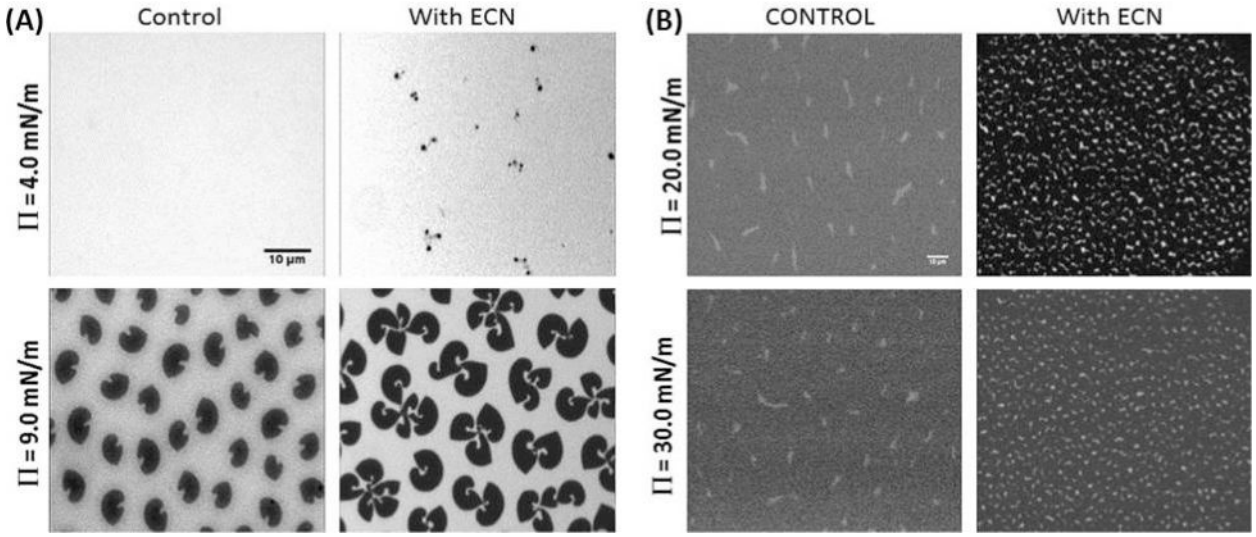

Figure 3.

Fluorescence microscopy images of pure (left) DPPC and (right) DPPG monolayers before (control) and after adding 1 wt % (10 μg/mL) ECN at two representative surface pressures. Contrast in these images is due to the selective segregation of bulky phospholipid-modified dye molecules into the more fluid regions. The kidney bean structures, characteristic of a pure DPPC system, underwent drastic transitions to a more spiral shape because of interactions with the ECNs. The scale bar is 10 μm.

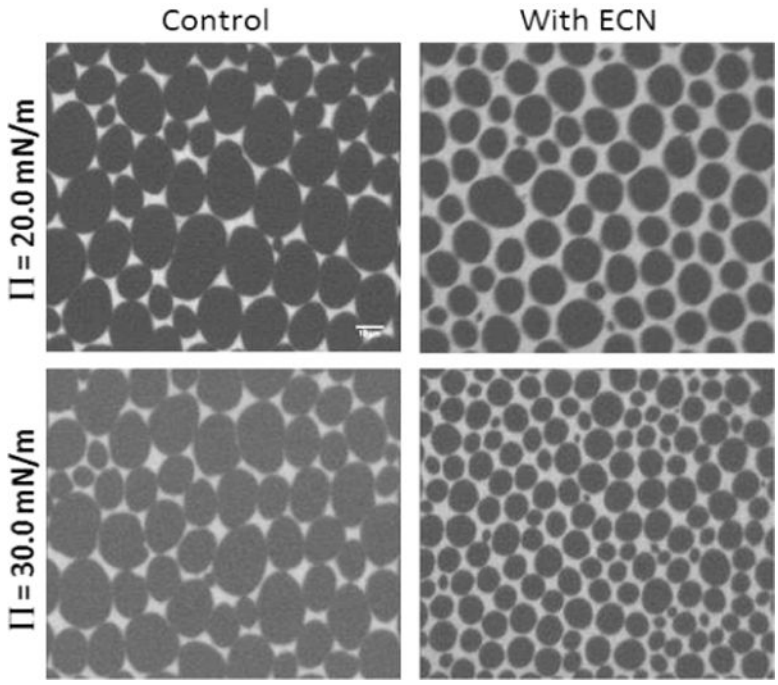

Figure 4.

Fluorescence microscopy images of a mixed DPPC:DPPG (75:25) monolayer with a net anionic charge before (control) and after adding 1 wt % (10 μg/mL) anionic ECNs. A decrease in the domain size and an increase in the number density were noted (Supporting Information Figure S1), but unlike a pure DPPC film, no change in the shape of the domains was observed. The scale bar is 10 μm.

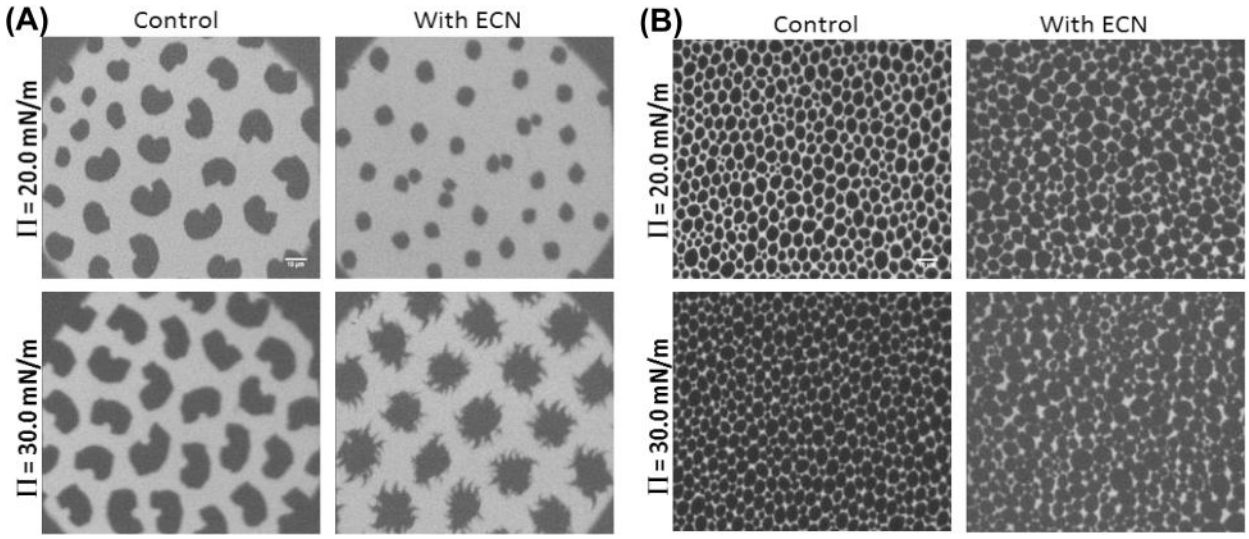

Figure 5.

Fluorescence microscopy images of a mixed (A) DPPC:POPC (7:3) monolayer with a net neutral charge and a (B) DPPC:POPG (7:3) monolayer with a net anionic charge and unsaturated lipids before (control) and after adding 1 wt % (10 μg/mL) anionic ECNs. The scale bar is 10 μm.

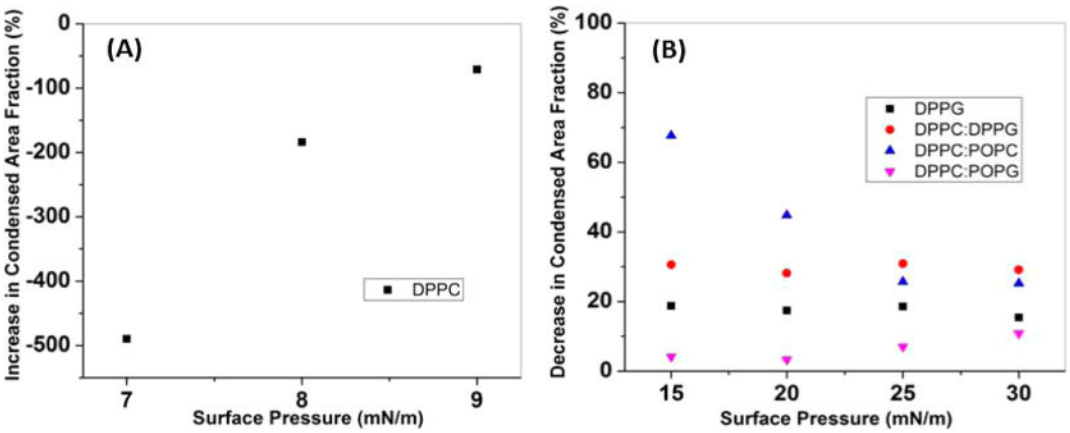

Figure 6.

Change in the condensed area fraction with the addition of ECN as a function of surface pressure. Positive values indicate a lowering in the area of the condensed region whereas a negative value refers to an increase in the area. (A) For DPPC, there was an increase in the domain area with the introduction of ECN, and the change decreased sharply with the increase in surface pressure. (B) In the case of DPPG, the condensed area fraction decreased as the negatively charged domains repelled the nanoparticles. A similar trend was observed for DPPC:DPPG. For DPPC:POPC, we recorded the highest reduction in area, but the change decreased with an increase in the surface pressure. Finally, we found very little change in the area for DPPC:POPG.

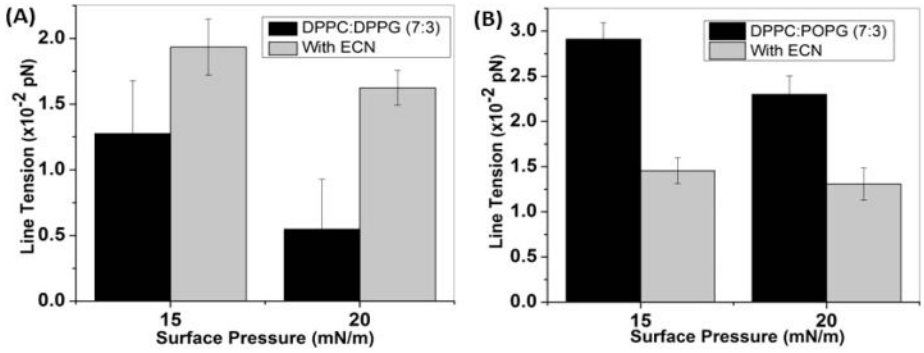

Figure 7.

Changes in the line tension of (A) DPPC:DPPG and (B) DPPC:POPG at two different surface pressures in the absence and presence of 1 wt % (10 μg/mL) ECN.

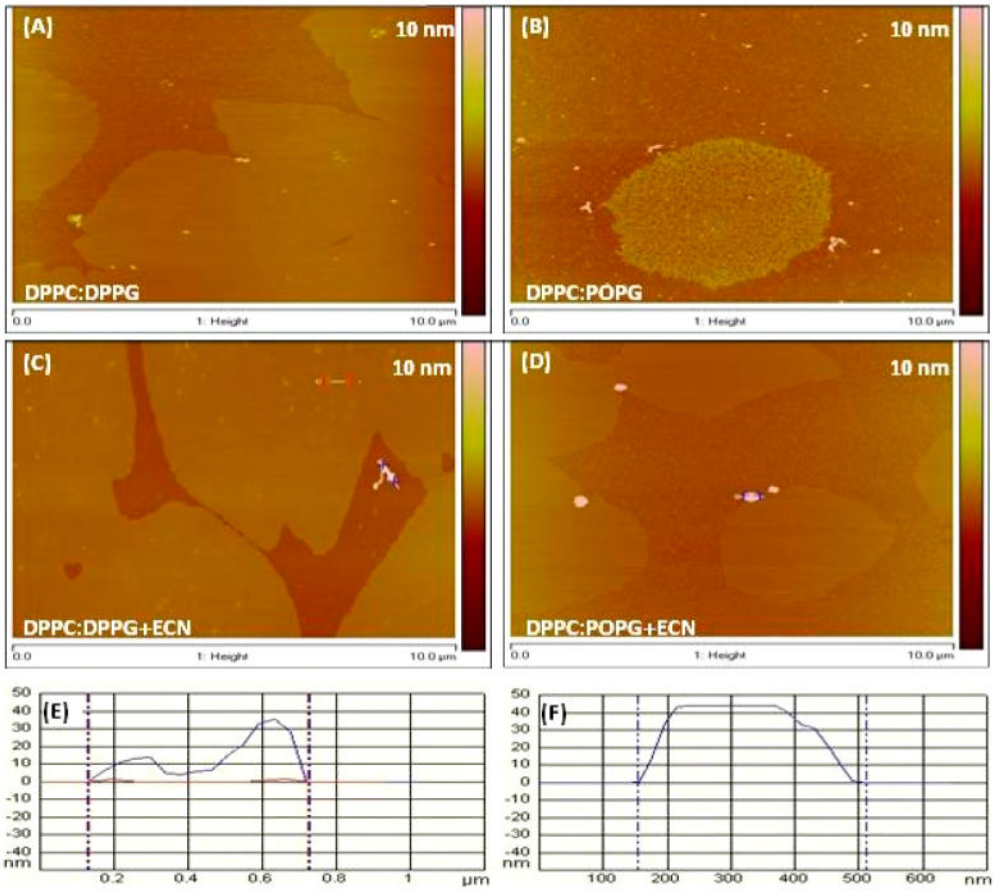

Figure 8.

AFM images of the net anionic binary mixtures of phospholipid films transferred onto a solid mica substrate. (A, C) DPPC:DPPG films in the absence and presence of ECN, respectively. (B, D) DPPC:POPG films in the absence and presence of ECN respectively. (E, F) Height analysis of the raised features indicated by white lines in C and D.